Original Article

Eur J Breast Health 2018; 14: 85-92
DOI: 10.5152/ejbh.2018.3829

Dual-Phase ADC Modelling of Breast Masses in Diffusion-Weighted Imaging: Comparison with Histopathologic Findings

Gökhan Ertaş[1], Can Onaygil[2], Onur Buğdaycı[3], Erkin Arıbal[4]

[1]Department of Biomedical Engineering, Yeditepe University, İstanbul, Turkey
[2]Institute of Diagnostic and Interventional Radiology, Oberlausitz-Kliniken gGmbH, Bautzen, Germany
[3]Department of Radiology, Marmara University School of Medicine, İstanbul, Turkey
[4]Department of Radiology, Acıbadem Altunizade Hospital, İstanbul, Turkey

ABSTRACT

Objective: To investigate the diagnostic value of dual-phase apparent diffusion coefficient (ADC) compared to traditional ADC values in quantitative diffusion-weighted imaging (DWI) for differentiating between benign and malignant breast masses.

Materials and Methods: Diffusion-weighted images of pathologically confirmed 88 benign and 85 malignant lesions acquired using a 3.0T MR scanner were analyzed. Small region-of-interests focusing on the highest signal intensity of lesions were used. Lesion ADC estimates were obtained separately from all b-value images (ADC; b=50, 400 and 800s/mm^2), lower b-value images (ADC_{low}; b=50 and 400s/mm^2) and higher b-value images (ADC_{high}; b=400 and 800s/mm^2). A set of dual-phase ADC (dpADC) models were constructed using ADC_{low}, ADC_{high} and a perfusion influence factor ranging from 0 to 1.

Results: Strong positive correlation is observable between ADC and all dpADCs (ρ=0.80-1.00). Differences in ADC and dpADCs between the benign and the malignant lesions are all significant ($p<0.05$). In detecting malignancy, traditional lesion ADC provides a good performance (AUC=89.9%) however $dpADC_{0.5}$ (dpADC with a factor of 0.5) accomplishes a better performance (AUC=90.8%). At optimal thresholds, ADC achieves 94.1% sensitivity, 72.7% specificity and 83.2% accuracy while $dpADC_{0.5}$ leads to 92.9% sensitivity, 79.5% specificity and 86.1% accuracy.

Conclusion: Dual-phase ADC modelling may improve the accuracy in breast cancer diagnosis using DWI. Further prospective studies are needed to justify its benefit in clinical setting.

Keywords: Breast, diffusion-weighted imaging, apparent diffusion coefficient, dual-phase

Cite this article as: Ertaş G, Onaygil C, Buğdaycı O, Arıbal E. Dual-Phase ADC Modelling of Breast Masses in Diffusion-Weighted Imaging: Comparison with Histopathologic Findings. Eur J Breast Health 2018; 14: 85-92.

Introduction

Diffusion-weighted imaging (DWI) utilizes diffusion signal attenuated due to the random microscopic motion of water molecules influenced by cell density, membrane integrity, tissue microstructure, perfusion and diffusion heterogeneity within the tissue (1). When compared with benign lesions and healthy tissue, more restricted water mobility of malignant lesions engenders slower attenuation of the diffusion signal captured from a set of images acquired with different degrees of diffusion weighting (reported as b-value) (2).

Quantitative diagnosis of cancer from DWI relies on metrics computed as the parameters of a "signal attenuation" model fitted to the diffusion signal data. The need for reliable and precise metrics motivates new studies on development of advanced models for better fittings to the diffusion signal data or advanced methods for optimized estimation of diffusion metrics (3). There exist several advanced exponential signal attenuation models such as stretched exponential (4), bi-exponential (known as intravoxel incoherent motion) (5), statistical (6) and kurtosis (7) capable of describing complex diffusion processes of the breast tissue. However, the parameters derived from these models are difficult to estimate and quite complex for use in diagnosis. For instance, physiological basis of the heterogeneity index of the stretched exponential model is reported to be uncertain and likewise pseudo-diffusion coefficient of the biexponential model is thought to be unreliable (8). On the other hand, these models involve several parameters that complicate both the diffusion estimation process and the diffusion weighted imaging protocol. To get accurate diffusion estimates, the initial value and the limits for any model parameter should be determined very carefully and an appropriate optimization method should be employed (9). To reach consistent numerical solutions, the number of b-values of the diffusion weighted imaging protocol must set to be more than the number of parameters in the model and

Address for Correspondence :
Gökhan Ertaş, e-mail: gokhan.ertas@yeditepe.edu.tr

Received: 18.10.2017
Accepted: 01.12.2017

large number of b-values would lengthen the imaging time remarkably making it unmanageable in clinical practice. These challenges promote the use of a mono-exponential model, that offers only one free parameter (namely apparent diffusion coefficient) estimated from two different b-value images with simplicity and high reproducibility, as the traditional model in diagnostic DWI in clinical practice (10).

Diffusion-weighted imaging and the use of apparent diffusion coefficient has been reported to be a very beneficial technique adjunct to dynamic contrast-enhanced imaging in diagnosis of breast cancer using magnetic resonance (MR) imaging (11, 12). While DWI holds potential to improve the detection and biological characterization of breast cancer (13), apparent diffusion coefficient (ADC) is capable of reflecting breast tissue cellularity, fluid viscosity, membrane permeability, macromolecular structures, microvascularity and lesion blood flow (14). Benign lesions have higher ADC than malignant lesions, especially the invasive carcinomas mainly due to their less compact cellularity (15). However, overlap between the ADC estimates from benign and malignant breast lesions motivate new studies to improve the performance of ADC in distinguishing benign lesions from malignant lesions.

The b-value set used during diffusion weighted imaging has an impact on the fitting performance of the mono-exponential model and on the diagnostic performance of ADC consequently (16). The lowest b-value is set to be sufficiently high so as the model can describe the diffusion signal data appropriately (b≥50s/mm^2 is usually used) while the highest b-value should be chosen so as to provide adequate suppression of water signal from normal fibroglandular tissue and maximum breast lesion visibility (17) (The use of b≥800s/mm^2 is usually recommended (18, 19)). Incorporating more than two b-values into the imaging protocol has been reported to provide more precise sampling of the diffusion signal and consistent ADC estimates (20, 21).

Diagnostic performance of ADC is also influenced by the methods used during image analysis and computation. A smaller region-of-interest (ROI) focusing on the highest signal intensity for the lesion is reported to have a better differential value for ADC when compared with a larger ROI for the overall lesion, especially in discrimination of invasive carcinomas (22). Normalized ADC (also called ADC ratio) calculated from the ratio of the lesion ADC to a reference tissue ADC (usually ipsilateral glandular breast tissue) is illustrated to make some improvements in the overall performance of ADC (23-25). Two separate ADCs from a lesion, one estimated from low b-value images and the other estimated from high b-value images, are demonstrated to be potentially more useful than a single lesion ADC in assessing the non-Gaussian water diffusion in vivo that is more closely related to the advanced models (26). In this study, we introduce dual-phase ADC modelling that integrates two separate ADCs, one from low b-value images and the other from high b-value images, and evaluate the utility of the modeling for breast masses in comparison with the histopathologic findings in quantitative DWI.

Materials and Methods

Patient Population

A total of one hundred seventy-three lesions (88 benign and 85 malignant) from 173 women aged 18-78 years (mean, 46 years), who underwent standard breast MRI including diffusion weighted imaging to clarify uncertain clinical, mammographic, sonographic findings or to assess preoperative staging of patients with known malignancies, have been retrospectively enrolled in this study. Written informed consent was obtained from each woman and local ethics committee approval was received. All findings were verified by histopathological examination. Average lesion size was 18.2±8.1mm. The benign lesions were 45 fibroadenomas, 14 columnar cell changes, 8 fibroses, 6 adenoses, 5 abscesses, 5 apocrine metaplasias and 5 other benign changes. The malignant lesions were 61 invasive ductal carcinomas, 9 invasive lobular carcinomas, 8 ductal carcinomas *in situ*, 3 invasive mucinous carcinomas, 1 invasive apocrine carcinoma, 1 medullary carcinoma, 1 medullary like carcinoma and 1 liposarcoma.

Breast MR Imaging Protocol

Breast MR imaging was performed by a 3T MR scanner (Magnetom Verio, Siemens Healthcare, Erlangen, Germany) using a dedicated 16-channel breast coil while patients were lying in prone position. At first, T2-weighted images were acquired using an axial turbo spin-echo with 70ms echo time (TE), 4100ms repetition time (TR), 448×381 matrix size, 320mm field of view (FOV), 3mm slice thickness. Next, diffusion-weighted images were captured in the axial plane using a 2D spin-echo echo-planar imaging (EPI) sequence at three b-values (b=50, 400 and 800s/mm^2) with the following parameters: 86ms echo time, 9700ms repetition time, 90° flip angle, 3 averages, 82×192 matrix size, 155×360mm FOV and 4mm slice thickness (leading to an in-plane resolution of 1.9×1.9×4mm^3). Finally, axial dynamic contrast-enhanced MR images were taken using 3D volumetric interpolated breath-hold (VIBE) imaging sequence with the following parameters: 1.77ms echo time, 5.01ms repetition time, 10° flip angle, 512×512 matrix size, 340mm FOV and 1mm slice thickness. During and immediately after the bolus injection of contrast agent Gadobutrol (0.1mmol/kg Gadovist®, Bayer Schering Pharma, Berlin, Germany) or Gadoterate Meglumine (0.1mmol/kg Dotarem®, Guerbet, Villepinte, France), one pre-contrast and six postcontrast bilateral images were acquired with a temporal resolution of 88 seconds.

Image Evaluation and ROI Delineation

All images acquired during imaging were transferred to workstation and evaluated by two experienced radiologists (with 4 and 17 years of experience in breast MRI, respectively) using Syngo. Via 3D reading and advanced visualization software (Siemens Healthcare, Erlangen, Germany) installed on the workstation. Both radiologists were blinded to pathology during evaluation. The radiologists first analyzed the dynamic contrast-enhanced images to localize lesions. The radiologists next evaluated each localized lesion on diffusion-weighted images and manually placed a region of interest (ROI) with consensus on the diffusion-weighted image with b=800s/mm^2 with care to include only the solid portion of the lesion with the highest signal intensity, excluding the necrotic and the cystic regions. All ROIs were defined to be circular with a diameter of 5mm. For each ROI placed, average signal intensity for each b-value of the diffusion-weighted imaging protocol given by the software was recorded for use to estimate apparent diffusion coefficients.

Dual-phase Apparent Diffusion Coefficient Modelling

Dual-phase ADC modelling integrates the two ADC estimates: ADC_{low} from lower b-value images (b=50-400s/mm^2) and ADC_{high} from higher b-value images (b=400-800s/mm^2) by using the following formula introduced in this study:

$$dpADC_{pf} = pf \times ADC_{low} + (1 - pf) \times ADC_{high} \quad (1)$$

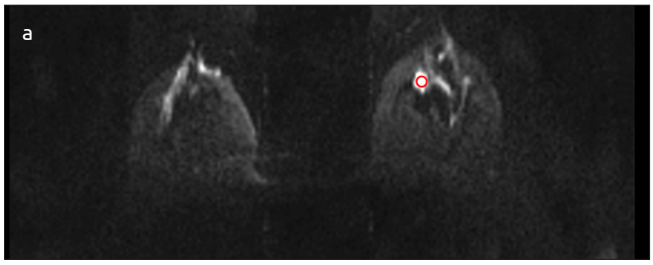

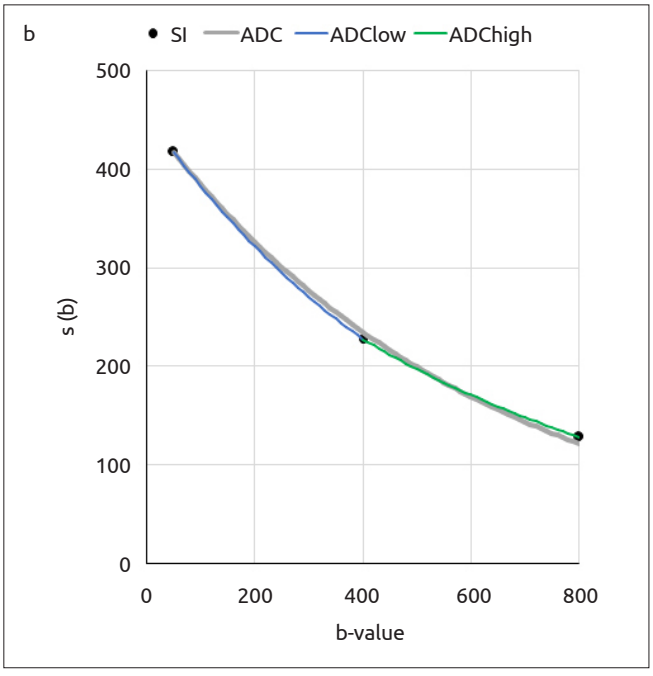

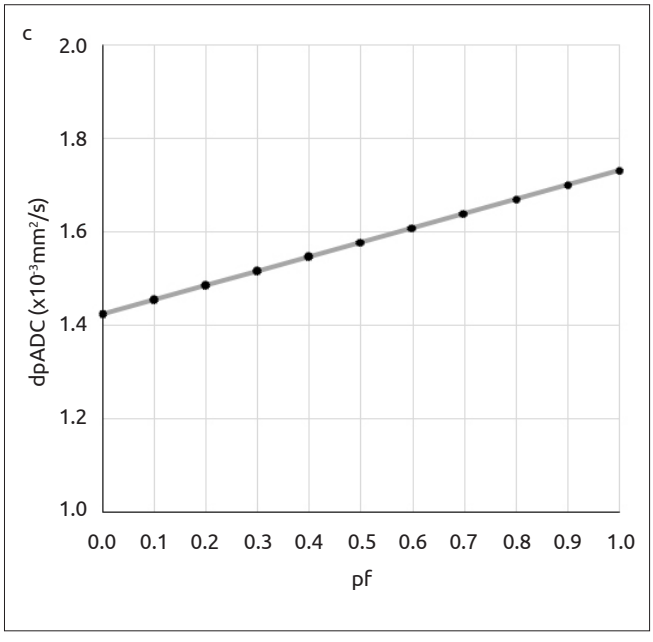

Figure 1. a-c. A 48-year-old woman with a benign lesion (a fibroadenoma) finding on the left breast and (a) the ROI placed for the lesion (solid red line contour) on the diffusion-weighted image at b=800mm^2/s. (b) Plots for the average signal intensity measurements recorded and for the results of the nonlinear fittings obtained (ADC=1.64×10^{-3}mm^2/s, ADC$_{low}$=1.73×10^{-3}mm^2/s and ADC$_{high}$=1.42×10^{-3}mm^2/s) and (c) Plot for the dpADC computed for a specific "perfusion" influence factor

Here pf is "perfusion" influence factor that ranges from 0 to 1. When pf is set to 0, the influence of ADC$_{low}$ is omitted giving dpADC$_0$ = ADC$_{high}$. In contrast, if pf is set to 1, the influence of ADC$_{high}$ is omitted and dpADC$_{1.0}$=ADC$_{low}$. ADC$_{low}$ is influenced by perfusion mostly and diffusion in a certain degree while ADC$_{high}$ reflects diffusion only. By voluntarily modifying the value of pf, different dual-phase ADC models can be obtained. The apparent diffusion coefficient can be estimated by using the mono-exponential model and the average signal intensity for an ROI recorded for n-th b-value of the diffusion-weighted image, S(b$_n$):

$$S(b_n) = S(b_1) \times \exp^{-b_n \times ADC} \quad (2)$$

In this study, ADC estimates were obtained for all breast lesions separately by using average signal intensity values from all b-value images (ADC; b=50, 400 and 800s/mm^2), from only lower b-value images (ADC$_{low}$; b=50 and 400s/mm^2) and from only higher b-value images (ADC$_{high}$; b=400 and 800s/mm^2). The estimations were performed using our own in-house developed computer software based on MatLab (Mathworks, Natick, MA) implementing a nonlinear fitting method based on the Trust-Region-Reflective least squares algorithm with the same pre-set initial value and the same limits for the ADC parameter (initial value=1.5×10^{-3}mm^2/s, upper and lower limits=3.0×10^{-3}mm^2/s and 0.3×10^{-3}mm^2/s, respectively) (Figure 1).

Statistical Analysis

Systematic difference in ADC and dpADC of the lesions were tested using Wilcoxon signed-ranks test. Spearman's rho (ρ) was used to test correlation between lesion dpADC and lesion ADC. Absolute relative difference between dpADC and ADC was measured using

$$\Delta_{rel} = \frac{|dpADC - ADC|}{ADC} \times 100 \quad (3)$$

Systematic differences in ADC and dpADC between benign and malignant lesions were tested using Mann-Whitney U-test. Diagnostic performance was assessed by plotting the receiver operating characteristic (ROC) curves and calculating the areas under the ROC curves (AUC). A p value of <0.05 was considered to be statistically significant.

Optimal thresholds for ADC and dpADC were determined by applying Youden statistics to the results of ROC analysis while considering improvements in both sensitivity and specificity. The classification performances of the optimal thresholds were assessed using sensitivity (Se), specificity (Sp), positive predictive value (PPV) and accuracy (Ac). All statistical analyses were performed using SPSS software for Windows (version 23; SPSS, Chicago, IL).

Results

Dual-phase apparent diffusion coefficient models using a set of perfusion influence factor (pf) and overall dual-phase ADC values (dpADC) estimated by the models from all breast lesions enrolled in this study are seen in Table 1. dpADC is at its minimum when pf is set to zero while dpADC is at its maximum when pf is set to one showing that dpADC is directly proportional to the perfusion influence factor: an increase in the factor leads to an increase in dpADC. ADC estimate from all lesions is 1.47±0.51×10^{-3}mm^2/s and a very similar value of 1.47±0.52×10^{-3}mm^2/s is obtained by the dpADC model with a pf of 0.7 leading to the lowest absolute relative difference among all the dpADC models studied (Δ_{rel}=1.6%). However, there are systematic difference in ADC and dpADC from all the models, but significant positive correlations are present between ADC and dpADC at all (p<0.05). Strong correlations exist between ADC and dpADC

obtained by the models using pf values of 0, 0.1 and 0.2 (ρ=0.80-0.90) but the rest of the models offer very strong correlations (ρ=0.90-1.00) (Figure 2). Table 2 shows the ADC and dpADC estimates from the benign and the malignant lesions. Independent of the perfusion influence fraction considered during modelling, low dpADC values indicate malignancy as in traditional ADC case. The differences in dpADC estimates between benign and malignant lesions from all the models are significant ($p<0.05$).

Table 1. Dual-phase ADC models and lesion dpADC with respect to perfusion influence factor and corresponding correlations and relative differences between dpADC and ADC

Model	pf	dpADC	ρ	Mean Δ_{rel}(%)
$dpADC_0$	0	1.31±0.61	0.80	20.4
$dpADC_{0.1}$	0.1	1.33±0.58	0.85	17.4
$dpADC_{0.2}$	0.2	1.36±0.56	0.88	14.3
$dpADC_{0.3}$	0.3	1.38±0.54	0.93	11.3
$dpADC_{0.4}$	0.4	1.40±0.52	0.96	8.2
$dpADC_{0.5}$	0.5	1.43±0.51	0.99	5.2
$dpADC_{0.6}$	0.6	1.45±0.51	1.00	2.1
$dpADC_{0.7}$	0.7	1.47±0.51	1.00	1.6
$dpADC_{0.8}$	0.8	1.49±0.52	0.99	4.0
$dpADC_{0.9}$	0.9	1.52±0.53	0.97	7.1
$dpADC_{1.0}$	1.0	1.54±0.55	0.94	10.1

Mean±SD in $10^{-3}mm^2/s$, overall ADC is (1.47 0.52)x$10^{-3}mm^2/s$
All statistical values are significant ($p<0.05$)
pf: perfusion influence factor; dpADC: dual-phase ADC; ρ: spearman's rho; Δ_{rel}: absolute relative difference

Table 2. Benign and malignant lesion dpADCs

Model	Benign Lesion	Malignant Lesion
$dpADC_0$	1.68±0.56 [a]	0.92±0.38
$dpADC_{0.1}$	1.70±0.52	0.95±0.35
$dpADC_{0.2}$	1.72±0.49	0.98±0.33
$dpADC_{0.3}$	1.73±0.46	1.00±0.31
$dpADC_{0.4}$	1.75±0.45	1.04±0.30
$dpADC_{0.5}$	1.76±0.44	1.07±0.30
$dpADC_{0.6}$	1.78±0.43	1.10±0.30
$dpADC_{0.7}$	1.80±0.44	1.13±0.32
$dpADC_{0.8}$	1.81±0.45	1.16±0.34
$dpADC_{0.9}$	1.83±0.48	1.19±0.34
$dpADC_{1.0}$	1.84±0.51	1.23±0.40

[a]Mean±SD in $10^{-3}mm^2/s$
All statistical values are significant ($p<0.05$)
dpADC: dual-phase ADC; ADC: apparent diffusion coefficient

Results of the ROC analyses of ADC and dpADC in differentiation of malignant lesions from benign lesions are as presented in Table 3. The dpADC models using a pf value of 0.2, 0.3, 0.4, 0.5 or 0.6 provides better performance (AUC≥90.0%) when compared to ADC (AUC=89.9%). Among these models, the model $dpADC_{0.5}$ that en-

Table 3. Diagnostic performance of dpADC and of ADC (in %)

			95% Confidence Interval of AUC	
	AUC	SE	Lower Bound	Upper Bound
$dpADC_{0.5}$	90.8	2.2	86.4	95.2
$dpADC_{0.4}$	90.7	2.3	86.3	95.2
$dpADC_{0.3}$	90.6	2.3	86.2	95.1
$dpADC_{0.6}$	90.3	2.3	85.7	94.8
$dpADC_{0.2}$	90.0	2.4	85.3	94.7
ADC	89.9	2.4	85.3	94.5
$dpADC_{0.7}$	89.7	2.4	85.0	94.3
$dpADC_{0.1}$	89.1	2.5	84.2	94.0
$dpADC_0$	88.1	2.6	82.9	89.9
$dpADC_{0.8}$	88.0	2.5	83.0	93.2
$dpADC_{0.9}$	86.2	2.7	80.8	91.5
$dpADC_{1.0}$	84.1	3.0	78.3	89.9

ADC: apparent diffusion coefficient; dpADC: dual-phase ADC; AUC: area under the curve; SE: standard error

Table 4. Classification performance of dpADC and of ADC

	Threshold[a]	False Detections	Se	Sp	PPV	Ac
$dpADC_{0.5}$	1.50	24 [18[b]+6[b]]	92.9	79.5	81.4	86.1
$dpADC_{0.6}$	1.54	25 [19+6]	92.9	78.4	80.6	85.5
$dpADC_{0.2}$	1.29	26 [14+12]	85.9	84.1	83.9	85.0
$dpADC_{0.3}$	1.33	26 [14+12]	85.9	84.1	83.9	85.0
$dpADC_{0.4}$	1.44	26 [18+8]	90.6	79.5	81.1	85.0
$dpADC_{0.1}$	1.35	28 [10+18]	88.2	79.5	80.6	83.8
ADC	1.61	29 [24+5]	94.1	72.7	76.9	83.2
$dpADC_{0.7}$	1.53	29 [12+17]	85.9	80.7	81.1	83.2
$dpADC_0$	1.13	30 [19+11]	77.6	87.5	85.7	82.7
$dpADC_{0.8}$	1.40	33 [18+15]	78.8	83.0	81.7	80.9
$dpADC_{0.9}$	1.42	35 [21+14]	75.3	84.1	82.1	79.8
$dpADC_{1.0}$	1.47	37 [21+16]	75.3	81.8	80	78.6

[a]In 10^{-3} mm^2/s
[b]Number of false positives and cNumber of false negatives
ADC: apparent diffusion coefficient; dpADC: dual-phase ADC; Se: sensitivity; Sp: specificity; PPV: positive predictive value; Ac: accuracy

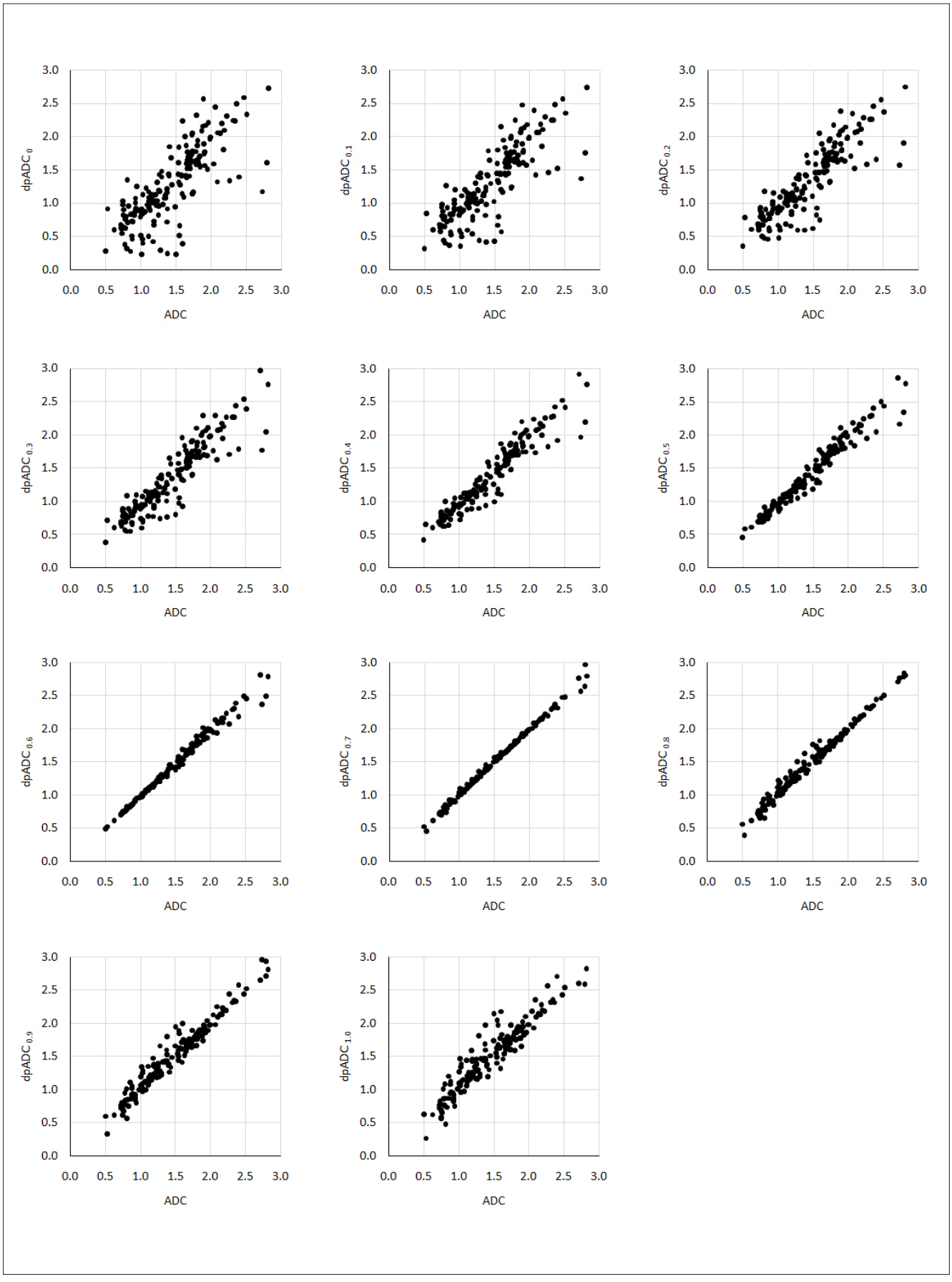

Figure 2. Plots for the ADC estimates with respect to dpADC estimates by the model using a pf of (a) 0, (b) 0.1, (c) 0.2, (d) 0.3, (e) 0.4, (f) 0.5, (g) 0.6, (h) 0.7, (i) 0.8, (j) 0.9 and (k) 1.0 from all lesions

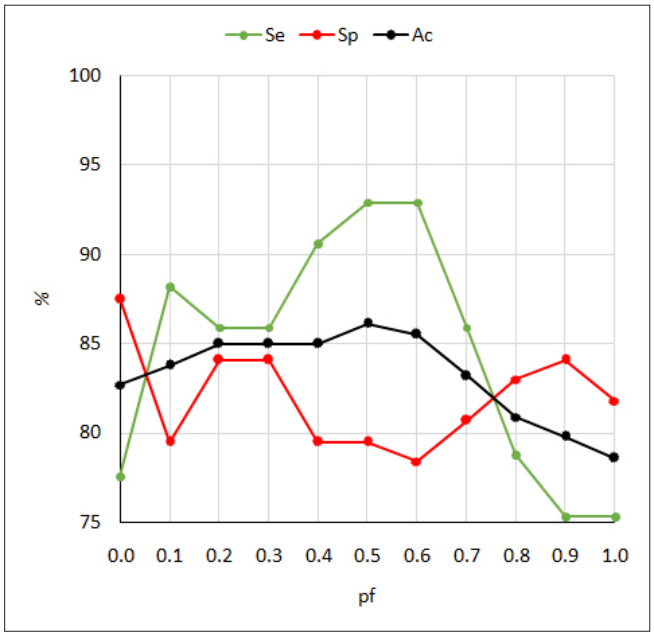

Figure 3. Plots for the sensitivity, specificity and overall accuracy of the dpADC models

rolls a perfusion influence fraction of 0.5 stands out in terms of its highest diagnostic accuracy (AUC=90.8%).

Diagnostic performances of ADC and dpADC form the models for optimal thresholds determined are listed in Table 4 and the corresponding plots for sensitivity, specificity and accuracy of the models are seen in Figure 3. ADC achieves 94.1% sensitivity, 72.7% specificity, 76.9% positive predictive value and 83.2% accuracy due to 5 false-negative and 24 false-positive detections (29 false detections in total) at an optimal threshold of $1.61\times10^{-3}mm^2/s$. Among the dpADC models, $dpADC_0$ offers low sensitivity (77.6%) but the highest specificity (87.5%) meanwhile $dpADC_{0.5}$ and $dpADC_{0.6}$ provide the highest sensitivity (92.9%) but lower specificities (79.5% and 78.4%, respectively). However, the best performance is given by $dpADC_{0.5}$: 92.9% sensitivity, 79.5% specificity, 81.4% positive predictive value and 86.1% accuracy due to 6 false-negative and 18 false-positive detections (24 false detections in total) at an optimal threshold of $1.50\times10^{-3}mm^2/s$. These results show that when compared to ADC, dual-phase ADC can provide almost the same sensitivity but considerably higher specificity that improves the positive predictive value and the accuracy.

Discussion and Conclusion

Challenges in quantitative diagnosis of breast cancer from diffusion-weighted imaging (DWI) motivate new studies to develop enhanced methods focusing on better modelling of the diffusion signal data and on enhancing the diagnostic performance of diffusion coefficients from the models. This study introduces a dual-phase apparent diffusion coefficient modeling that may improve the dialogistic performance of traditional ADC in breast cancer.

The dual-phase apparent diffusion coefficient model integrates two separate ADCs: one from low b-value images ($b=50\text{-}400s/mm^2$) and the other from high b-value images ($b=400\text{-}800s/mm^2$) of DWI. The model estimates a single diffusion coefficient value (dpADC) by summing the two ADCs weighted by a perfusion influence factor. The value of the factor may range from 0 to 1 and different dpADC estimates can be obtained by using different factor values. In the current study, analyses are performed using the factor values of 0, 0.1, 0.2, 0.3, 0.4, 0.5, 0.6, 0.7, 0.8, 0.9 and 1.0.

A meta-analysis of thirteen studies evaluating the diagnostic performance of ADC in quantitative breast DWI from 964 lesions (615 malignant and 349 benign) demonstrates that pooled mean ADC from malignant lesions is significantly lower than that of benign lesions that may range from 0.87 to $1.61\times10^{-3}mm^2/s$ and the recommended ADC threshold for cancer diagnosis may vary from 0.90 to $1.76\times10^{-3}mm^2/s$ (27). In the current study, ADC estimations are performed by nonlinear fitting the mono-exponential model to average lesion signal intensity data to ensure high precision in the estimates (use of commonly preferred linear fitting complemented with log transformation in ADC estimations is reported to lower the precision (28)). The mean malignant lesion ADC and the optimal ADC threshold for cancer diagnosis are found to be $1.12\times10^{-3}mm^2/s$ and $1.61\times10^{-3}mm^2/s$, respectively, all in agreement with the literature. The optimal ADC threshold leads to misclassification of 29 lesions (24 benign and 5 malignant lesions) from 173 lesions (88 malignant and 85 benign) analyzed.

Mean dpADC from the malignant lesions is significantly lower than that of benign lesions independent of the perfusion influence factor used in the model that demonstrates a possible use of dual-phase ADC modelling in cancer diagnosis. The dual-phase ADC model with a perfusion influence factor of 0.5 offers the best performance among all the models. From this model, the mean malignant lesion dpADC is $1.07\times10^{-3}mm^2/s$ and the optimal dpADC threshold for cancer diagnosis is $1.50\times10^{-3}mm^2/s$. The model misclassifies 24 lesions (18 benign and 6 malignant lesions) from the 173 breast lesions analyzed.

One invasive ductal carcinoma, 1 liposarcoma, 1 ductal carcinoma in situ and 2 invasive mucinous carcinoma are misclassified by both ADC and dpADC. Use of dpADC lead to misclassification of one invasive lobular carcinoma additionally. On the other hand, 5 fibroadenomas, 4 abscesses, 3 adenoses, 2 columnar cell changes, 3 fibroses and 1 intraductal papilloma are misclassified by both ADC and dpADC. Use of ADC resulted in misclassification of other 6 benign lesions: 3 fibroadenomas, 1 abscess, 1 apocrine metaplasia and 1 columnar cell change. Dual-phase ADC modelling reduces the number of false-positive detections remarkably.

Some precautions should be considered for dpADC. Although dpADC of malignant lesions is significantly lower than that of benign lesions, mucinous carcinoma can reveal high dpADC values and can be misdiagnosed as benign while papilloma, abscess and fibrosis may demonstrate low dpADC values and therefore can be misdiagnosed as cancer. These shortcomings can be due to the underlying pathophysiology of these specific lesions. The mucinous carcinoma is among the malignant lesions, but it may reveal low cellularity and with relatively high-water content (29). Also, abscess, papilloma, and fibrosis are the benign lesions that may exhibit high cellularity (30). The current study imaging protocol schedules DWI before DCE-MRI scan and in the case of DWI immediately after DCE-MRI, presence of contrast agent in the tissue may lead to an artificial increase in dpADC from malignant lesions (A similar artificial increase has been recognized for ADC (30)).

During this retrospective study, a dedicated post-processing software has been developed and used to obtain the two separate ADC estimates within the dual-phase ADC model. However, the vendor-specif-

ic software packages installed on the main MR consoles are equipped with functionality to obtain different ADC maps (3) and can be set-up with little effort to obtain the maps required for dpADC modelling. This would facilitate the use of dpADC in clinic practice.

There are some limitations of the current study. The clinical utility of the dpADC for multi-centers and the repeatability and reproducibility of the dpADC from different brand MR scanners are questionable since this study enrolls breast lesions imaged using a 3.0T MR scanner at a single center. Small region-of-interests are placed for the breast lesions manually. This process requires utmost attention and experience especially for the lesions obscured with architectural distortion and if not performed precisely, may lead to a great variability in dpADC. The value of dpADC is calculated using two different ADC estimates and three different b-value images from DWI. More precise calculations can be accomplished with more number of images acquired with well selected b-values (20, 21). The current study has been designed to assess the best dpADC model in differentiating the breast masses using DWI only. Its use in clinical setting and value in multiparametric imaging complemented with dynamic contrast-enhanced MR imaging should be evaluated with further prospective studies.

In conclusion, dual-phase ADC modelling can provide almost the same sensitivity but considerably better specificity than traditional ADC calculations. Thus, dual-phase ADC modelling can improve the diagnostic accuracy of quantitative DWI in differentiating breast cancers from benign lesions. Requiring acquisition of only three different b-value images and benefiting from easy-to-setup ADC mapping tools installed on the main MR console, dpADC based evaluations can be easily adoptable to current imaging and evaluation protocols. Further prospective studies considering multiple institutions and multiple scanners are needed to justify its benefit in clinical setting and its value in diagnosis of breast lesions.

Ethics Committee Approval: Ethics committee approval was received for this study from the ethics committee of Marmara University School of Medicine.

Informed Consent: Written informed consent was obtained from patients who participated in this study.

Peer-review: Externally peer-reviewed.

Author Contributions: Concept - G.E., E.A.; Design - G.E., C.O.; Supervision - G.E., E.A., C.O.; Resources - G.E., E.A., C.O., O.B.; Materials - E.A., C.O., O.B.; Data Collection and/or Processing - E.A., C.O., O.B.; Analysis and/or Interpretation - G.E., E.A.; Literature Search - G.E., E.A.; Writing Manuscript - G.E.; Critical Review - E.A.

Conflict of Interest: No conflict of interest was declared by the authors.

Financial Disclosure: The authors declared that this study has received no financial support.

References

1. Koh DM and Padhani AR. Diffusion-weighted MRI: a new functional clinical technique for tumour imaging. Br J Radiol 2006; 79: 633-635. (PMID: 16793851) [CrossRef]
2. Padhani AR, Liu G, Koh DM, Chenevert TL, Thoeny HC, Takahara T, Dzik-Jurasz A, Ross BD, Van Cauteren M, Collins D, Hammoud DA, Rustin GJ, Taouli B, Choyke PL. Diffusion-weighted magnetic resonance imaging as a cancer biomarker: consensus and recommendations. Neoplasia 2009; 11: 102-125. (PMID: 19186405) [CrossRef]
3. Koh DM, Collins DJ. Diffusion-weighted MRI in the body: applications and challenges in oncology. AJR Am J Roentgenol.2007; 188: 1622-1635. (PMID: 17515386) [CrossRef]
4. Mazaheri Y, Afaq A, Rowe DB, Lu Y, Shukla-Dave A, Grover J. Diffusion-weighted magnetic resonance imaging of the prostate: improved robustness with stretched exponential modelling. J Comput Assist Tomogr 2012; 36: 695-703. (PMID: 23192207) [CrossRef]
5. Le Bihan D, Breton E, Lallemand D, Aubin M-L, Vignaud J, Laval-Jeantet M. Separation of diffusion and perfusion in intravoxel incoherent motion MR imaging. Radiology 1988; 168: 497-505. (PMID: 3393671) [CrossRef]
6. Yablonskiy DA, Bretthorst GL, Ackerman JJ. Statistical model for diffusion attenuated MR signal. Magn Reson Med 2003; 50: 664-669. (PMID: 14523949) [CrossRef]
7. Jensen JH, Helpern JA, Ramani A, Lu H, Kaczynski K. Diffusional kurtosis imaging: the quantification of non-gaussian water diffusion by means of magnetic resonance imaging. Magn Reson Med 2005; 53: 1432-1440. (PMID: 15906300) [CrossRef]
8. Panek R, Borri M, Orton M, O'Flynn E, Morgan V, Giles SL, deSouza N, Leach MO, Schmidt MA. Evaluation of diffusion models in breast cancer. Med Phys 2015; 42: 4833-4839. (PMID: 26233210) [CrossRef]
9. Suo S, Lin N, Wang H, Zhang L, Wang R, Zhang S, Hua J, Xu J. Intravoxel incoherent motion diffusion-weighted MR imaging of breast cancer at 3.0 tesla: Comparison of different curve-fitting methods. J Magn Reson Imaging 2015; 42: 362-370. (PMID: 25407944) [CrossRef]
10. Le Bihan D. Apparent diffusion coefficient and beyond: what diffusion MR imaging can tell us about tissue structure. Radiology 2013; 268: 318-322 (PMID: 23882093). [CrossRef]
11. Park SH, Choi HY, Hahn SY. Correlations between apparent diffusion coefficient values of invasive ductal carcinoma and pathologic factors on diffusion-weighted MRI at 3.0 Tesla. J Magn Reson Imaging 2015; 41: 175-182. (PMID: 24353241) [CrossRef]
12. Sharma U, Sah RG, Agarwal K, Parshad R, Seenu V, Mathur SR, Hari S, Jagannathan NR. Potential of diffusion-weighted imaging in the characterization of malignant, benign, and healthy breast tissues and molecular subtypes of breast cancer. Frontiers in Oncology 2016; 6: 126. (PMID: 27242965) [CrossRef]
13. Partridge SC, Nissan N, Rahbar H, Kitsch AE, Sigmund EE. Diffusion-weighted breast MRI: Clinical applications and emerging techniques. J Magn Reson Imaging 2017; 45: 337-355. (PMID: 27690173) [CrossRef]
14. Costantini M, Belli P, Rinaldi P, Bufi E, Giardina G, Franceschini G, Petrone G, Bonomo L. Diffusion-weighted imaging in breast cancer: relationship between apparent diffusion coefficient and tumour aggressiveness. Clin Radiol 2010; 65: 1005-1012. (PMID: 21070905) [CrossRef]
15. Woodhams R, Ramadan S, Stanwell P, Sakamoto S, Hata H, Ozaki M, Kan S, Inoue Y. Diffusion-weighted Imaging of the Breast: Principles and Clinical Applications. Radiographics 2011; 31: 1059-1084. (PMID: 21768239) [CrossRef]
16. Peters NH, Vincken KL, van den Bosch MA, Luijten PR, Mali WP, Bartels LW. Quantitative diffusion weighted imaging for differentiation of benign and malignant breast lesions: the influence of the choice of b-values. J Magn Reson Imaging 2010; 31: 1100-1105. (PMID: 20432344) [CrossRef]
17. Koh DM, Collins DJ, Orton MR. Intravoxel incoherent motion in body diffusion-weighted MRI: reality and challenges. AJR Am J Roentgenol 2011; 196: 1351-1361. (PMID: 21606299) [CrossRef]
18. Ochi M, Kuroiwa T, Sunami S, Murakami J, Miyahara S, Nagaie T, Oya M, Yabuuchi H, Hatakenaka M. Diffusion-weighted imaging (b value=1500 s/mm2) is useful to decrease false-positive breast cancer cases due to fibrocystic changes. Breast Cancer 2013; 20: 137-144. (PMID: 22161277) [CrossRef]
19. Min Q, Shao K, Zhai L, Liu W, Zhu C, Yuan L, Yang J. Differential diagnosis of benign and malignant breast masses using diffusion-weighted magnetic resonance imaging. World J Surg Oncol 2015; 13: 32. (PMID: 25889380) [CrossRef]

20. Malayeri AA, El Khouli RH, Zaheer A, Jacobs MA, Corona-Villalobos CP, Kamel IR, Macura KJ. Principles and applications of diffusion-weighted imaging in cancer detection, staging, and treatment follow-up. Radiographics 2011; 31: 1773-1791. (PMID: 21997994) [CrossRef]
21. Pereira SC, Martins G, Carvalhaes de Oliveira Rde V. Diffusion magnetic resonance imaging of the breast. Magn Reson Imaging Clin N Am 2011; 19: 95-110. (PMID: 21129637) [CrossRef]
22. Arponent O, Sudah M, Masarwah A, Taina M, Rautiainen S, Könönen M, Sironen R, Kosma VM, Sutela A, Hakumäki J, Vanninen R. Diffusion-weighted imaging in 3.0 Tesla breast MRI: Diagnostic performance and tumor characterization using small subregions vs. whole tumor regions of interest. PLoS One 2015; 10: e0138702. (PMID: 26458106) [CrossRef]
23. El Khouli RH, Jacobs MA, Mezban SD, Huang P, Kamel IR, Macura KJ, Bluemke DA. Diffusion-weighted imaging improves the diagnostic accuracy of conventional 3.0-T breast MR imaging. Radiology 2010; 256: 64-73. (PMID: 20574085) [CrossRef]
24. Şahin C, Arıbal E. The role of apparent diffusion coefficient values in the differential diagnosis of breast lesions in diffusion-weighted MRI. Diagn Interv Radiol 2013; 19: 457-462. (PMID: 24004972)
25. Zhao J, Guan H, Li M, Gu H, Qin J, Wu X. Significance of the ADC ratio in the differential diagnosis of breast lesions. Acta Radiol 2016; 57: 422-429. (PMID: 26071495) [CrossRef]
26. Tachibana Y, Omatsu T, Kishimoto R. Efficacy of multiple b-value DWI analysis to detect changes in cervical cancer of uterine while charged particle radiation therapy. 2014; DOI: 10.1594/ecr2014/C-1318.
27. Chen X, Li WL, Zhang YL, Wu Q, Guo YM, Bai ZL. Meta-analysis of quantitative diffusion-weighted MR imaging in the differential diagnosis of breast lesions. BMC Cancer 2010; 10: 693. (PMID: 21189150) [CrossRef]
28. Veraart J, Sijbers J, Sunaert S, Leemans A, Jeurissen B. Weighted linear least squares estimation of diffusion MRI parameters: strengths, limitations, and pitfalls. NeuroImage 2013; 81: 335-346. (PMID: 23684865) [CrossRef]
29. Woodhams R, Kakita S, Hata H, Iwabuchi K, Umeoka S, Mountford CE, Hatabu H. Diffusion-weighted imaging of mucinous carcinoma of the breast: evaluation of apparent diffusion coefficient and signal intensity in correlation with histologic findings. Am J Roentgenol 2009; 193: 260-266. (PMID: 19542422) [CrossRef]
30. Partridge SC, McDonald ES. Diffusion weighted MRI of the breast: Protocol optimization, guidelines for interpretation, and potential clinical applications. Magn Reson Imaging Clin N Am 2013; 21: 601-624. (PMID: 23928248) [CrossRef]